Supporting Information

Asymmetric iron–titanium pairs within ultrathin TiO_2 nanosheet enable high-efficiency nitrate reduction to ammonia

Supplementary Figures

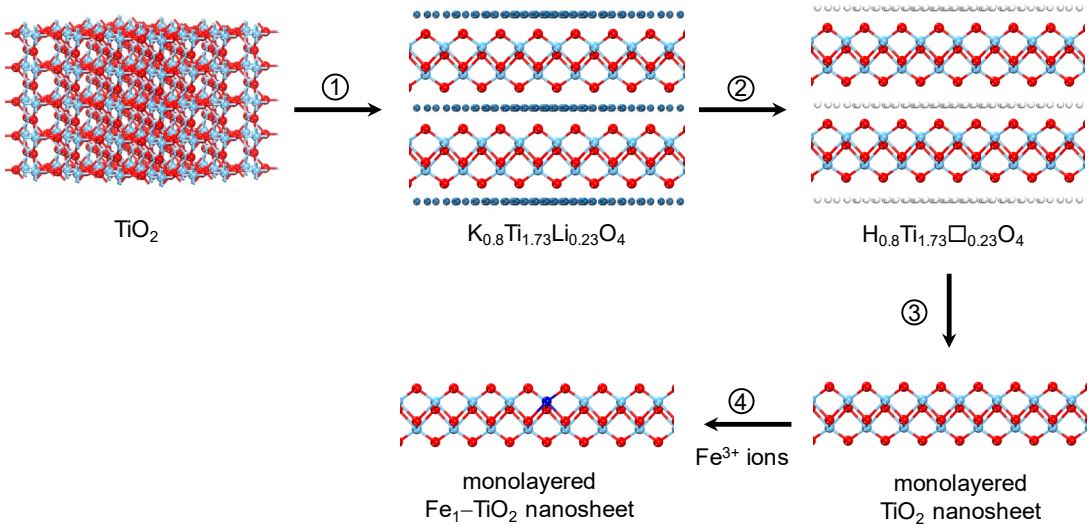

Fig. S1. Schematic diagram of the synthetic procedure of Fe_1–TiO_2 nanosheet. Blue, cyan and red balls represent Fe, Ti and O atoms, respectively.

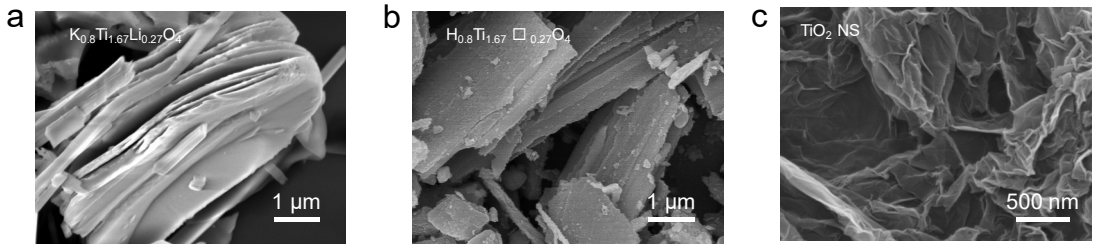

Fig. S2. (a) SEM image of $K_{0.8}Ti_{1.67}Li_{0.23}Fe_{0.1}O_4$ nanosheet. (b) SEM image of $H_{0.8}Ti_{1.67}\square_{0.23}Fe_{0.1}O_4$ nanosheet.

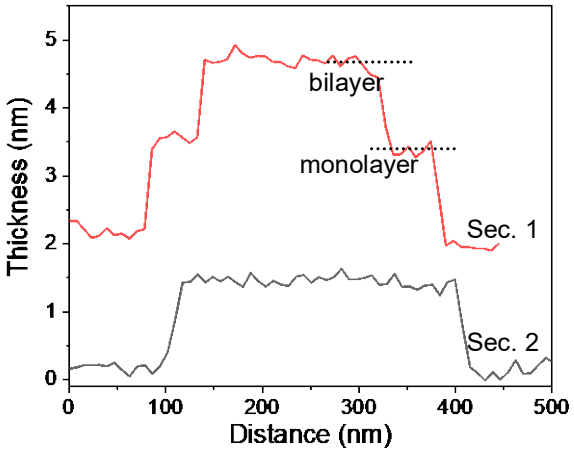

Fig. S3. The corresponding thickness of the marked sections in Fig. 1c.

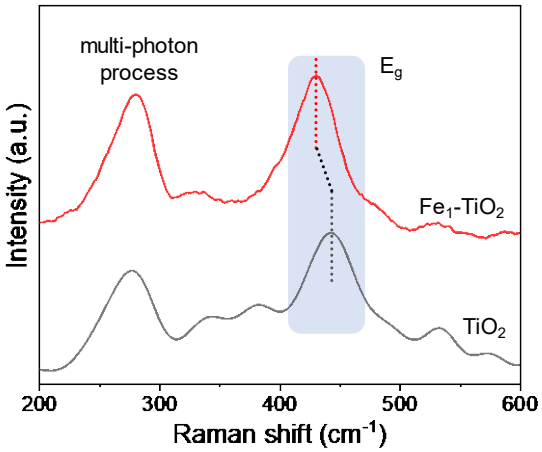

Fig. S4. Raman spectra of Fe_1-TiO_2 and TiO_2 nanosheet.

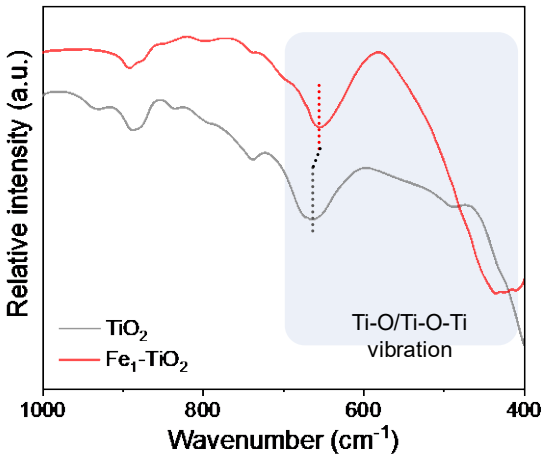

Fig. S5. Infrared spectrogram of Fe_1-TiO_2 and TiO_2 nanosheet.

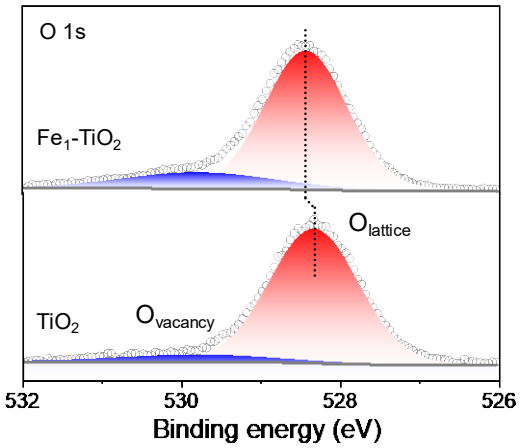

Fig. S6. XPS spectra of Fe_1-TiO_2 and TiO_2 nanosheet in the O 1s regions.

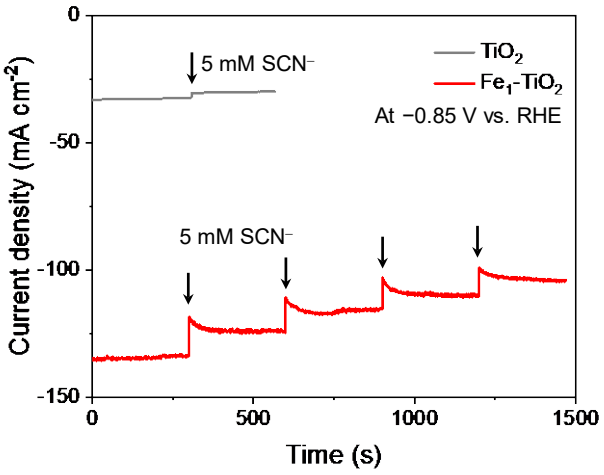

Fig. S7. The current density collected at –0.85 V vs. RHE for Fe_1–TiO_2 and TiO_2 upon the addition of KSCN.

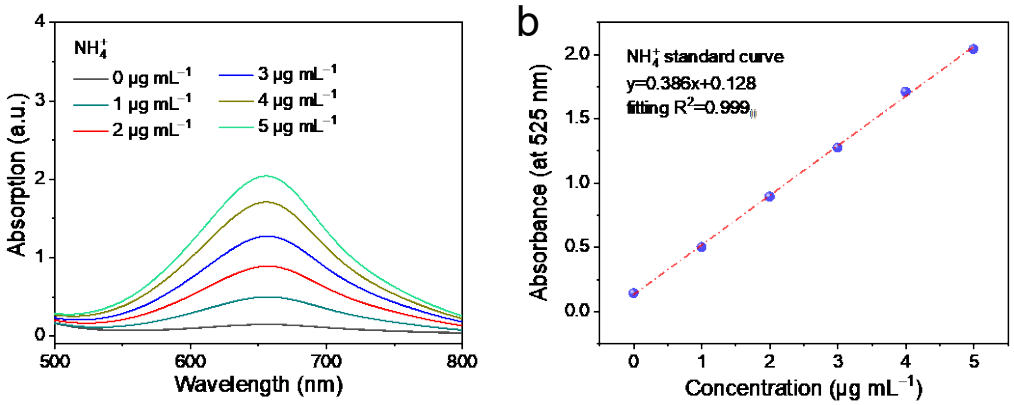

Fig. S8. The standard adsorption spectra of ammonia (a) and their linear fitting (b).

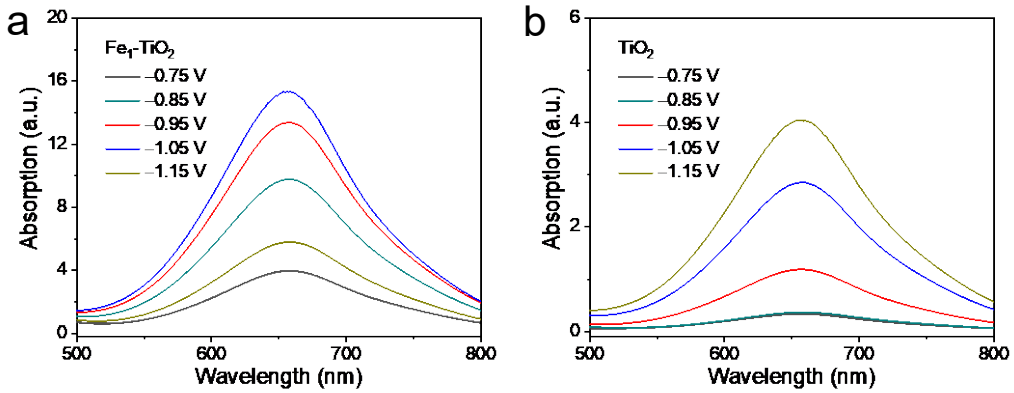

Fig. S9. (a) The adsorption spectra of ammonia after NRA on Fe_1-TiO_2 nanosheet at each given potential. (b) The adsorption spectra of ammonia after NRA on TiO_2 nanosheet at each given potential.

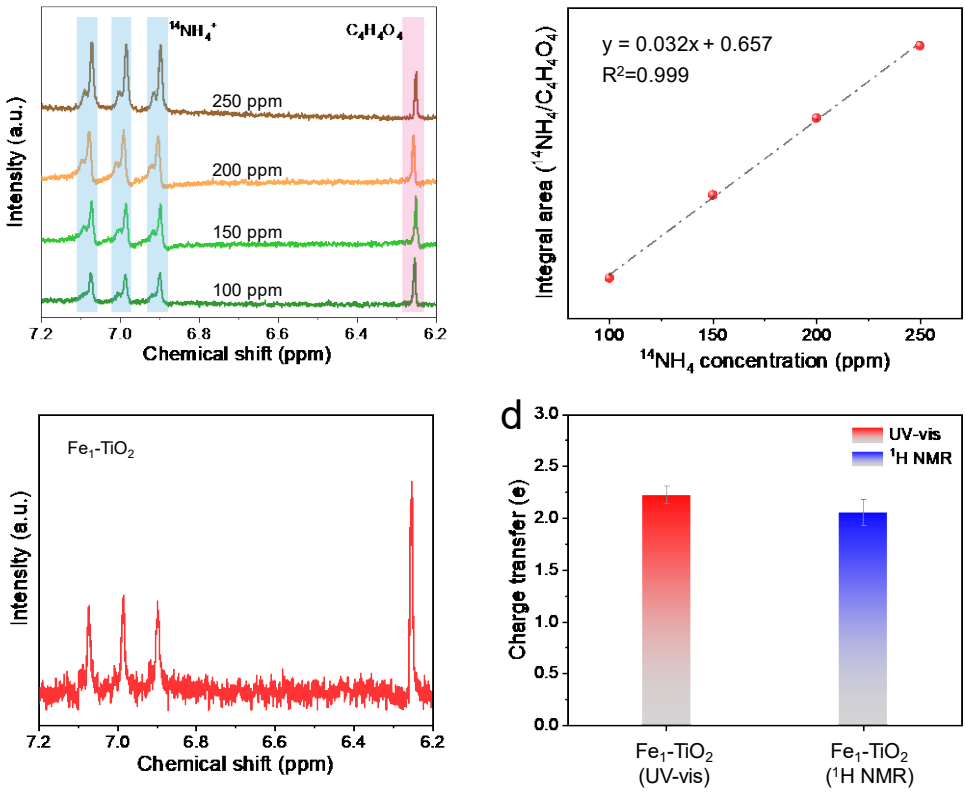

Fig. S10. The standard ^{1}H NMR spectra of $^{14}NH_4^+$ at various concentration (a) and their linear fitting (b). (c) The ^{1}H NMR spectrum of the product obtained by electrocatalysis for 2 hours at –0.85 V vs. RHE.

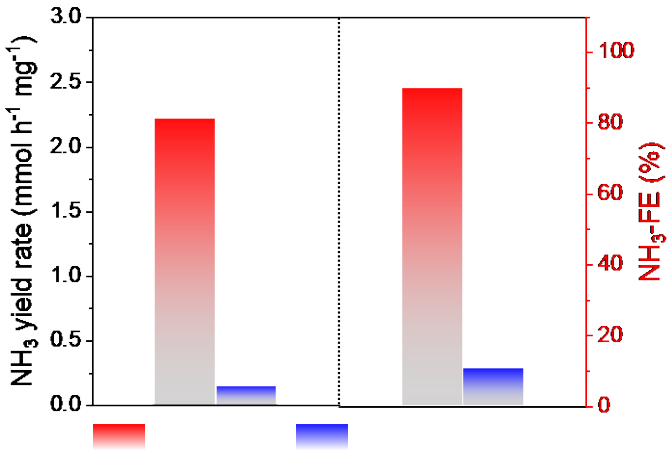

Fig. S11. NH_3 yields rate and FEs of Fe_1-TiO_2 and TiO_2 nanosheet at –0.85V.

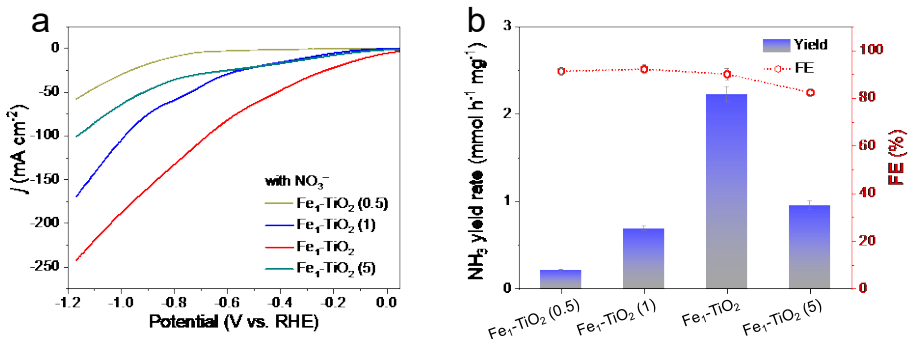

Fig. S12. NH_3 yields rate and FEs of Fe_1-TiO_2 with varied Fe loading amount. The collected LSV curves (a) and the corresponding FEs and ammonia yield rates (b) for Fe_1-TiO_2 (0.5), Fe_1-TiO_2 (1), Fe_1-TiO_2 and Fe_1-TiO_2 (5).

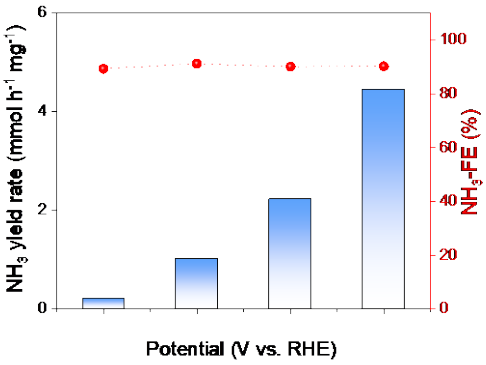

Fig. S13. The corresponding FEs and ammonia yield rates for Fe_1-TiO_2 when varying the concentration of nitrate at 0.01, 0.05, 0.1 and 0.5 M.

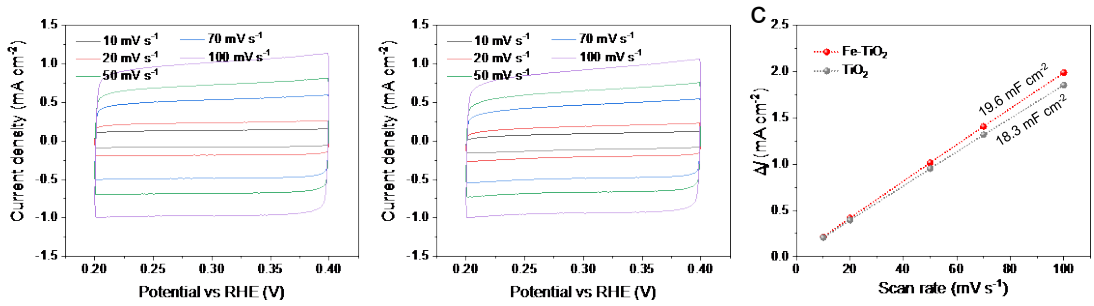

Fig. S14. CV curves obtained at various scan rates at non-Faradic potential windows for Fe_1–TiO_2 (a) and TiO_2 (b). The extracted ECSA of Fe_1–TiO_2 and TiO_2 from Fig. S11a and b.

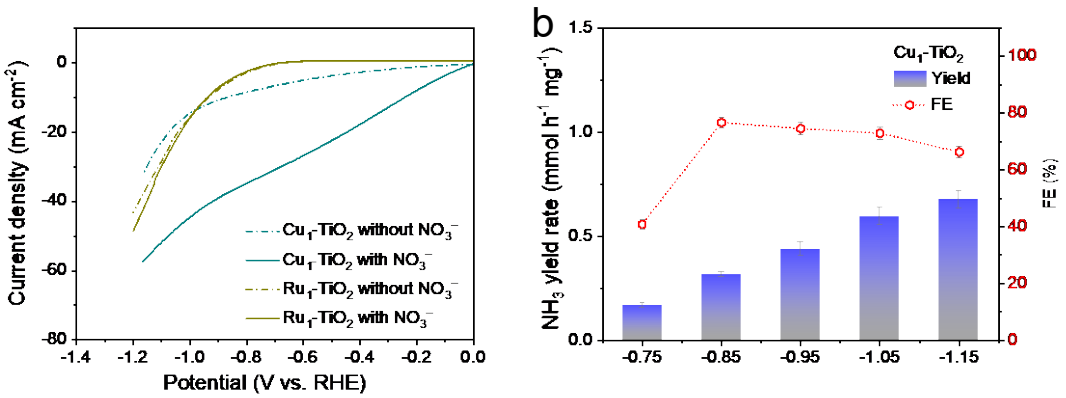

Fig. S15. (a) The collected LSV curves of Cu_1-TiO_2 and Ru_1-TiO_2 at the conditions of with and without nitrate. (b) The corresponding FEs and ammonia yield rates for Cu_1-TiO_2 at different potentials.

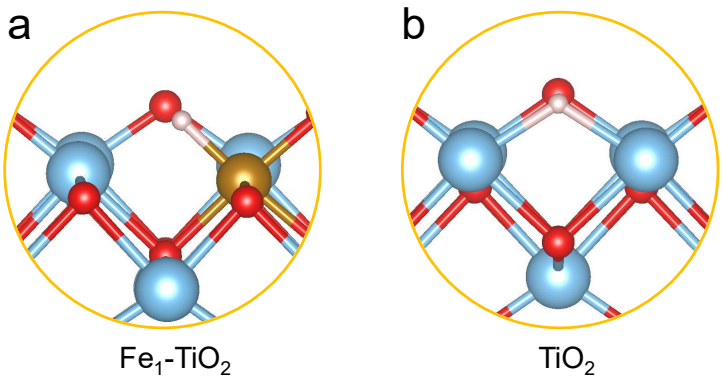

Fig. S16. Atomic arrangement diagram of Fe_1-TiO_2 (a) and TiO_2 (b) nanosheet upon adsorption of proton.

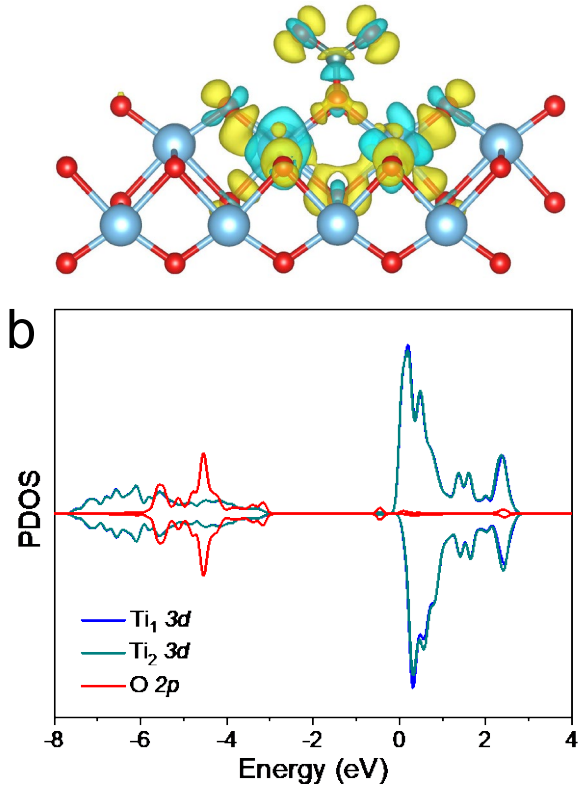

Fig. S17. (a) The differential charge density for TiO_2 interface. Cyan and yellow isosurfaces (at level of 0.01 e $Bohr^{-3}$) represent electron depletion and accumulation, and light blue, red, and green spheres denote the Ti, O, and nitrate atoms, respectively. (b) Projected DOS (pDOS) profile of TiO_2 nanosheet upon adsorption of nitrate.

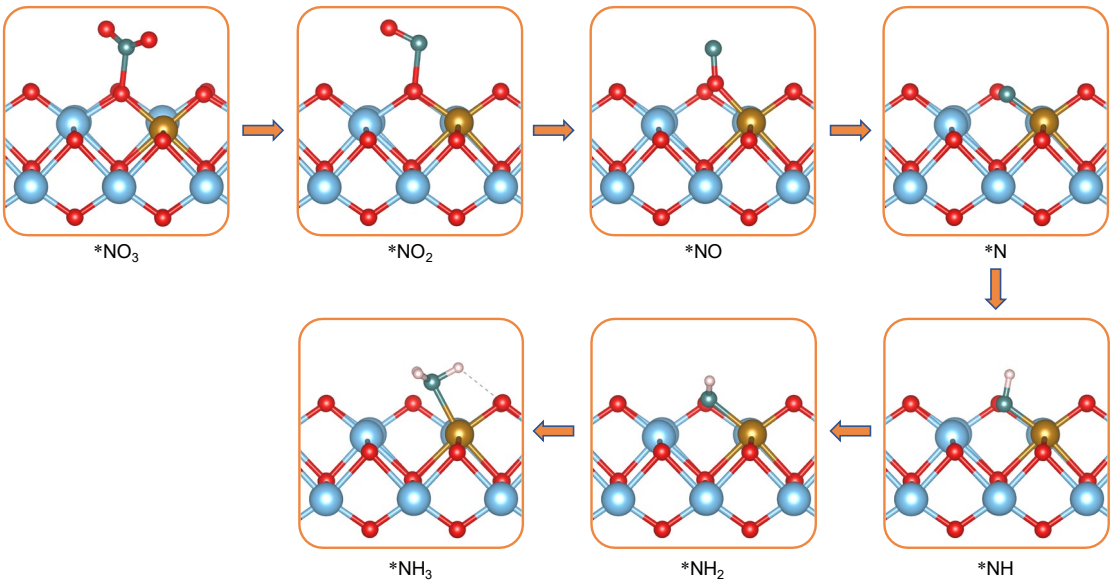

Fig. S18. The involved intermediates for nitrate reduction over Fe_1–TiO_2.

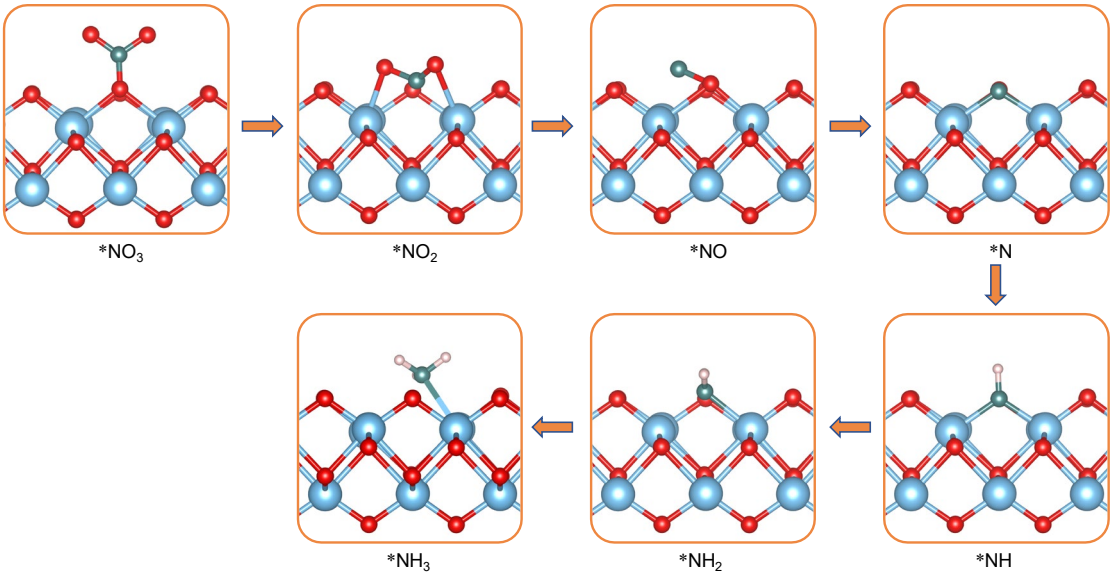

Fig. S19. The involved intermediates for nitrate reduction over TiO_2.

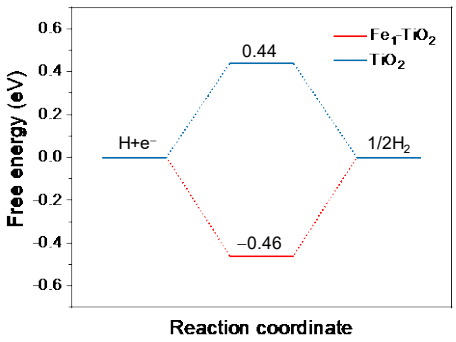

Fig. S20. The calculated Gibbs free energy of hydrogen evolution over Fe_1–TiO_2 and TiO_2.

Table S1. Structural parameters of Fe_1–TiO_2 extracted from the EXAFS fitting. (S_0^2=0.8). The C.N. represents coordination number.

Sample	Scattering pair	C.N.	R (Å)	σ^2 (10^{-3}Å^2)	ΔE_0 (eV)
Fe_1–TiO_2	Fe–O	5.2 ± 0.5	1.94 ± 0.02	6.0 ± 1.5	–4.9 ± 1.6

S_0^2 is the amplitude reduction factor S_0^2=0.8. C.N., R, σ^2 and ΔE_0 are coordination number, scattering distance, Debye-Waller factor, and edge-energy shift, respectively.

Table S2. Comparison of nitrate-reduction performance of Fe_1–TiO_2 with the reported catalysts in the previously literatures.

Sample	FE_{NH3}	Yield Rate	Potential vs. RHE	Ref.
Fe_1–TiO_2	97.4%	2.2 mmol h^{-1} mg^{-1} 0.62 mmol h^{-1} cm^{-2}	–0.85 V	This work
Co/TiO_2 NSs	97.4%	0.22 mmol cm^{-2} h^{-1}	–0.72 V	1
FeOOH/CP	92%	901 μg h^{-1} cm^{-2}	−0.5 V	2
FeCoNiAlTi	95.23%	0.52 mg h^{-1} cm^{-2}	−0.5 V	3
MPS–Cu NDs/CF	94.43%	0.22 mmol h^{-1} cm^{-2}	−1.2 V vs. SCE	4
F–NFs/CF	81.5%	602.8 μg h^{-1} cm^{-2}	–0.54 V	5
Cu_2O–NCs	92.9%	56.2 mg h^{-1} mg_{cat}^{-1}	–0.85 V	6
10Cu/TiO_{2-x}	81.34%	0.11 mmol h^{-1} mg^{-1}	–0.75 V	7
a–RuO_2	97.46%	0.12 mmol h^{-1} cm^{-2}	–0.35 V	8
Cu_2O	85.26%	0.07 mmol h^{-1} mg^{-1}	−1.2 V vs. Ag/AgCl	9
Zn/Cu–2.3		5.8 mol g^{-1} h^{-1}	–0.85 V	10
Co_3O_4/Co–h	88.7 %	0.26 mmol h^{-1} cm^{-2}	−0.8 V	11
TiO_{2-x}	85.0%	0.05 mmol h^{-1} mg^{-1}	−1.6 V vs. SCE	12
V−Cu NAE	95.1%	7.85 mg h^{-1} cm^{-2}	−0.3 V	13
Cu nanotubes	85.7%	778.6 μg h^{-1} mg^{-1}	−1.3 V vs. SCE	14
Fe@Cu_1FeO_x	95.4%	1.98 mg h^{-1} cm^{-2}	−1.3 V vs. SCE	15
Co−Fe@Fe_2O_3	85.2%	0.88 mg h^{-1} cm^{-2}	−0.75 V	16
Fe SAC	75%	0.52 mg h^{-1} $mg_{cat.}^{-1}$	−0.66 V	17
Fe–PPy SACs	~100%	2.75 mg h^{-1} cm^{-2}	−0.7 V	18
Pd–TiO_2	92.1%	0.07 mmol cm^{-2} h^{-1}	−0.7 V	19
TiO_{2-x}	78.0%	0.10 mmol cm^{-2} h^{-1}	−1.0 V	20

References

1. Y.-T. Xu, Y. Han, D. K. Sam and Y. Cao, *J. Mater. Chem. A*, 2022, **10**, 22390-22398.
2. Q. Liu, Q. Liu, L. Xie, Y. Ji, T. Li, B. Zhang, N. Li, B. Tang, Y. Liu and S. Gao, *ACS Appl. Mater. Interfaces*, 2022, **14**, 17312-17318.
3. R. Zhang, Y. Zhang, B. Xiao, S. Zhang, Y. Wang, H. Cui, C. Li, Y. Hou, Y. Guo and T. Yang, *Angew Chem Int. Ed.*, 2024, e202407589.
4. Z. Yu, J. Xie, T. Ren, H. Yu, K. Deng, Z. Wang, H. Wang, L. Wang and Y. Xu, *Inorg. Chem.*, 2023, **62**, 16228-16235.
5. W. Zhang, Y. Yao, Z. Chen, S. Zhao, F. Guo and L. Zhang, *Environ. Sci. Technol.*, 2024, **58**, 7208-7216.
6. X.-H. Wang, Z.-M. Wang, Q.-L. Hong, Z.-N. Zhang, F. Shi, D.-S. Li, S.-N. Li and Y. Chen, *Inorg. Chem.*, 2022, **61**, 15678-15685.
7. X. Zhang, C. Wang, Y. Guo, B. Zhang, Y. Wang and Y. Yu, *J. Mater. Chem. A*, 2022, **10**, 6448-6453.
8. Y. Wang, H. Li, W. Zhou, X. Zhang, B. Zhang and Y. Yu, *Angew Chem Int. Ed.*, 2022, **134**, e202202604.
9. Z. Gong, W. Zhong, Z. He, Q. Liu, H. Chen, D. Zhou, N. Zhang, X. Kang and Y. Chen, *Appl. Catal. B-Environ.*, 2022, **305**, 121021.
10. L. Wu, J. Feng, L. Zhang, S. Jia, X. Song, Q. Zhu, X. Kang, X. Xing, X. Sun and B. Han, *Angew Chem Int. Ed.*, 2023, **135**, e202307952.
11. F. Zhao, G. Hai, X. Li, Z. Jiang and H. Wang, *Chem. Eng. J.*, 2023, **461**, 141960.
12. R. Jia, Y. Wang, C. Wang, Y. Ling, Y. Yu and B. Zhang, *ACS Catal.*, 2020, **10**, 3533-3540.
13. B. Zhang, Z. Dai, Y. Chen, M. Cheng, H. Zhang, P. Feng, B. Ke, Y. Zhang and G. Zhang, *Nat. Commun.*, 2024, **15**, 2816.
14. C. Li, S. Liu, Y. Xu, T. Ren, Y. Guo, Z. Wang, X. Li, L. Wang and H. Wang, *Nanoscale*, 2022, **14**, 12332-12338.
15. B. Zhou, L. Yu, W. Zhang, X. Liu, H. Zhang, J. Cheng, Z. Chen, H. Zhang, M. Li and Y. Shi, *Angew Chem Int. Ed.*, 2024, e202406046.
16. S. Zhang, M. Li, J. Li, Q. Song and X. Liu, *P. Natl. Acad. Sci.*, 2022, **119**, e2115504119.
17. Z.-Y. Wu, M. Karamad, X. Yong, Q. Huang, D. A. Cullen, P. Zhu, C. Xia, Q. Xiao, M. Shakouri, F.-Y. Chen, J. Y. Kim, Y. Xia, K. Heck, Y. Hu, M. S. Wong, Q. Li, I. Gates, S. Siahrostami and H. Wang, *Nat. Commun.*, 2021, **12**, 2870.
18. P. Li, Z. Jin, Z. Fang and G. Yu, *Energy Environ. Sci.*, 2021, **14**, 3522-3531.
19. Y. Guo, R. Zhang, S. Zhang, Y. Zhao, Q. Yang, Z. Huang, B. Dong and C. Zhi, *Energy Environ. Sci.*, 2021, **14**, 3938-3944.
20. Z. Wei, X. Niu, H. Yin, S. Yu and J. Li, *Appl. Catal. A-Gen.*, 2022, **636**, 118596.